ACOUSTIC RIDGE WAVEGUIDE TECHNOLOGY

Robert S. Wagers

Texas Instruments, Incorporated

Prepared for:

Office of Naval Research
Advanced Research Projects Agency

August 1975

ACOUSTIC RIDGE WAVEGUIDE TECHNOLOGY

Robert S. Wagers

Texas Instruments Incorporated

August 1975

Semiannual Technical Report

6 January 1975 - 30 June 1975

Sponsored by

Advanced Research Projects Agency

ARPA Order No. 2827

The views and conclusions contained in this document are those of the authors and should not be interpreted as necessarily representing the official policies, either expressed or implied, of the Advanced Research Projects Agency or the U. S. Government.

TI Report No.
08-75-30

ACOUSTIC RIDGE WAVEGUIDE TECHNOLOGY

Contract No. N00014-75-C-0317

Robert S. Wagers

Texas Instruments Incorporated

August 1975

Semiannual Technical Report

6 January 1975 - 30 June 1975

Sponsored by
Advanced Research Projects Agency
ARPA Order No. 2827

ARPA Order Number:	2827
Program Code Number:	5D10
Name of Contractor:	Texas Instruments Incorporated Central Research Laboratories P. O. Box 5936 Dallas, Texas 75222
Effective Date of Contract:	6 January 1975
Contract Expiration Date:	29 November 1975
Amount of Contract:	$68,219
Contract Number:	N00014-75-C-0317
Principal Investigator and Phone No.:	Robert S. Wagers (214) 238-5238
Scientific Officer:	Director, Electronic and Solid State Sciences Program Physical Sciences Division Office of Naval Research 800 N. Quincy Street Arlington, Virginia 22217
Short Title of Work:	Acoustic Waveguides

TECHNICAL REPORT SUMMARY

This report presents results obtained during the first six months of development of acoustic waveguides. A primary motivation for developing acoustic waveguides is to take advantage of the potential size reduction over current surface acoustic wave technology. Waveguide components represent the next step in microminiaturization of acoustic signal processing devices. Devices that may be developed include directional couplers, ring resonators, and serial memory. In addition, because of the high degree of spatial confinement of the acoustic energy, nonlinear and acousto-optic interactions become possible.

The technical problems associated with this development are twofold: (1) development of suitable etching processes for waveguide formation, and (2) development of fine geometry stencils for transducer fabrication.

- Waveguide Formation

A suitable etching process for waveguide formation in α-quartz has been developed. A quartz wafer masked off with sputtered metal films can be etched in boiling hydrofluoric acid to produce wedge-shaped waveguides. Waveguide etching in higher coupling materials, such as lithium niobate, is currently not a developed process. The problem in lithium niobate etching is maintaining uniformity of the waveguide cross section. We have results showing that the nonuniform etching is related to crystal defects, polishing inadequacy, and metal etch mask adhesion. All of these problems are being examined.

- Transducer Fabrication

Stencils are being fabricated by orientation-dependent etching of silicon. The stencils will be used in conjunction with standard electron beam metal evaporation techniques to produce the transducer patterns. This procedure

for transducer fabrication is being considered rather than photoresist and wet etching of the metals because of the difficulties introduced by the surface tension of the photoresist when it is applied to the edge of a waveguide. The processes required for orientation-dependent etching of silicon are well known at Texas Instruments, and development of the stencils is proceeding without difficulty.

No special equipment has been purchased or developed on this contract.

TABLE OF CONTENTS

LIST OF ILLUSTRATIONS

LIST OF ILLUSTRATIONS
(continued)

SECTION I

INTRODUCTION

This report presents results obtained during the first six months of development of acoustic waveguides. Section I outlines the motivation for the work and the objectives being pursued. In Section II results obtained from low frequency prototype waveguides are evaluated. Section III discusses our present status in the development of etched waveguides on $LiNbO_3$ and α quartz. Plans for future work are given in Section IV.

A. Objectives

A primary motivation for developing acoustic waveguides is to take advantage of the potential size reduction from current surface acoustic wave (SAW) technology. In addition, because of the high degree of spatial confinement of the acoustic energy, nonlinear and acousto-optic interactions become possible. Devices that may be developed include directional couplers, ring resonators, and serial memories.

B. Approach to Waveguide Development

The basic configuration under development is shown in Figure 1. This configuration was chosen over other alternatives for two principal reasons: (1) the fundamental mode of the ideal structure is dispersionless; and (2) when the structure is fabricated on a wafer as shown, the flexure and electric potentials of the guide are compatible with transducer fabrication in the plane of the wafer's top surface. Development of a delay line with the configuration of Figure 1 breaks down into two major divisions, fabrication of the waveguide and fabrication of the transducers.

1. Waveguide Fabrication

Orientation-dependent etching (ODE) of crystals has been demonstrated in many materials. Notably, silicon, exhibits preferential etching, and a vast

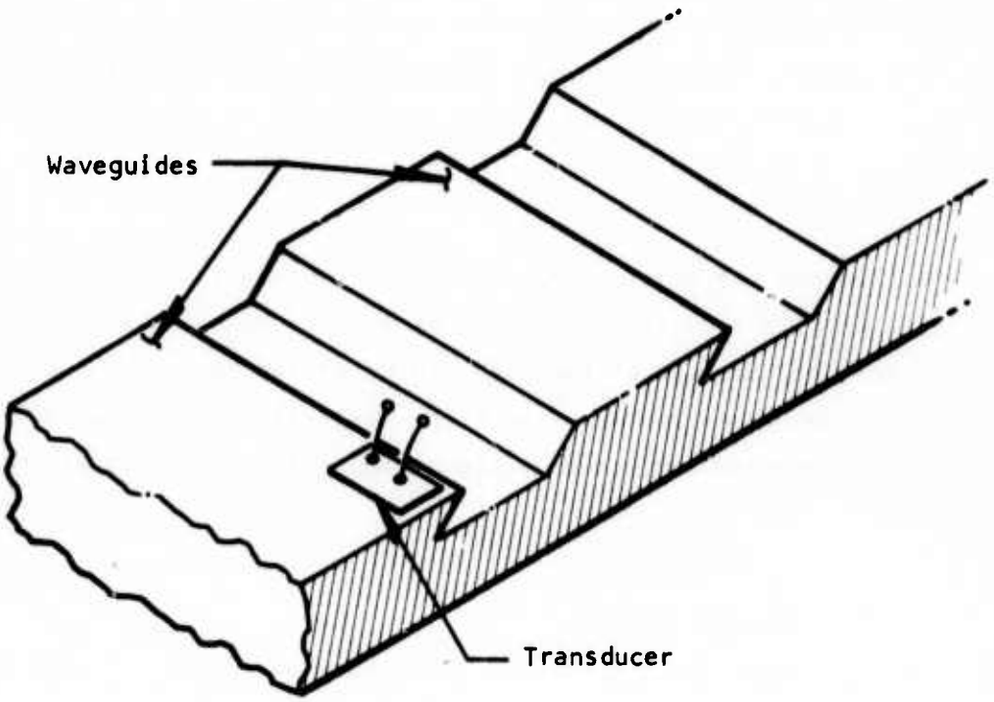

Figure 1 Acoustic Waveguides on a Piezoelectric Wafer. The overhanging wedge-shaped structures confine and guide the wave. Transducers are fabricated on the face of the waveguide that is coplanar with the top surface of the wafer.

body of literature has been produced dealing with ODE of silicon. Unfortunately, silicon is not piezoelectric, and while waveguides may be easily formed[1] in the material, transduction is an exceedingly difficult problem.

Quartz and $LiNbO_3$ also permit preferential etching. While no body of literature on ODE of these two materials exists, Texas Instruments, through the work of Dr. D. F. Weirauch,[2] has developed considerable expertise during the past year in etching device geometries in quartz and $LiNbO_3$. It is this ODE capability that enables us to consider the configuration of Figure 1. Our current work on ODE of $LiNbO_3$ and quartz is discussed in Section III.

2. Transducer Fabrication

Optimal transducer design includes not only defining a process that produces coupling metallizations on the waveguides, but also takes into account spurious mode discrimination and fundamental mode impedance matching considerations. Work directed toward obtaining guidelines with regard to these problems is being done in parallel with the etching activities. The transducer work has been carried out on a low frequency (1 MHz) prototype device that was mechanically cut and polished from a block of piezoelectric ceramic. This work, which is essentially complete, is discussed in Section II.

High frequency waveguides will require fine metallizations for the transducers. To produce such patterns, we are developing silicon stencil fabrication techniques.[3] A discussion of this activity is given in Section IV, Future Work.

SECTION II

PROTOTYPE DEVICE STUDIES

A. Introduction

Prototype waveguides were built to evaluate the spurious mode excitation problem and to obtain quantitative data on transducer impedances. Previous work on waveguides on $LiNbO_3$ showed that the modes excited by the transducer pads could easily be stronger than the desired waveguide mode.

The waveguides were fabricated from a ceramic, Glennite G-1408. Since this material is similar to PZT-4, we used the already published[4] dispersion and coupling data shown in Figure 2 in evaluating our results. (The specifications supplied for the Glennite ceramic were not sufficiently complete to permit dispersion and coupling calculations.)

Top angles of all waveguides were about 33°, and the lateral surfaces of 0.75 inch and 0.89 inch were polished until porosity of the material was the factor limiting surface quality. Approximately 3.5 inches of free propagation path was available, and on the tested units, apex roughness throughout the propagation path was less than 0.04 wavelength peak-to-peak.

B. Spurious Modes

Schematic representations of the transducers tried for excitation of the ceramic waveguides are shown in Figure 3. Figure 3(a) shows a grating mode configuration with a ground plane on the lower surface of the waveguide. Figures 3(b) and 3(c) illustrate interdigital transducers. The transducers in Figures 3(a) and 3(c) were 9.5 λ long with equal-width stripes and spaces, while the transducer in Figure 3(b) was 5 λ long. All the masks were designed for 1 MHz operation with 1.0 inch of free propagation between the last finger of the input

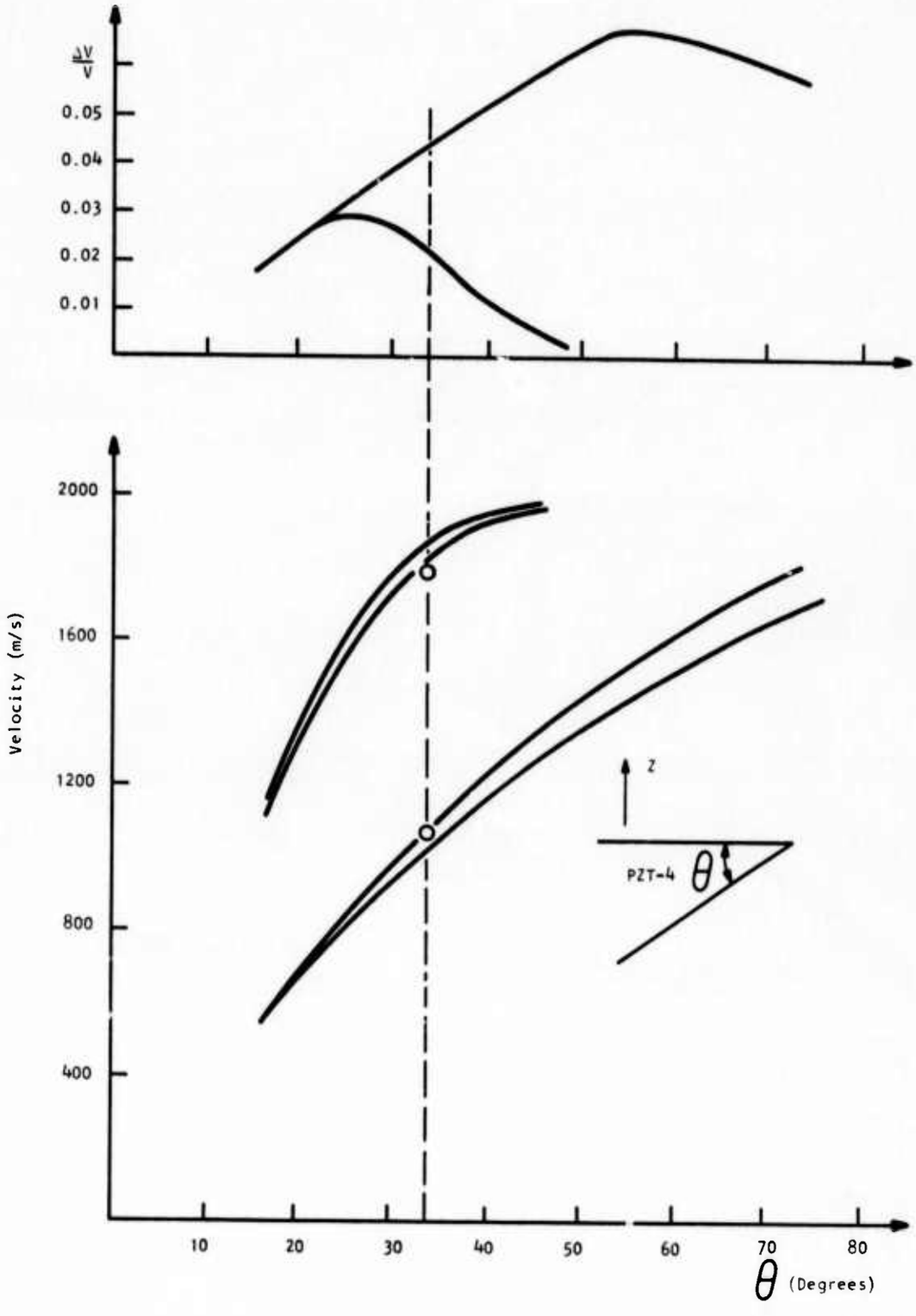

Figure 2 Phase Velocity and Coupling for PZT-4 (From Lagasse[4])

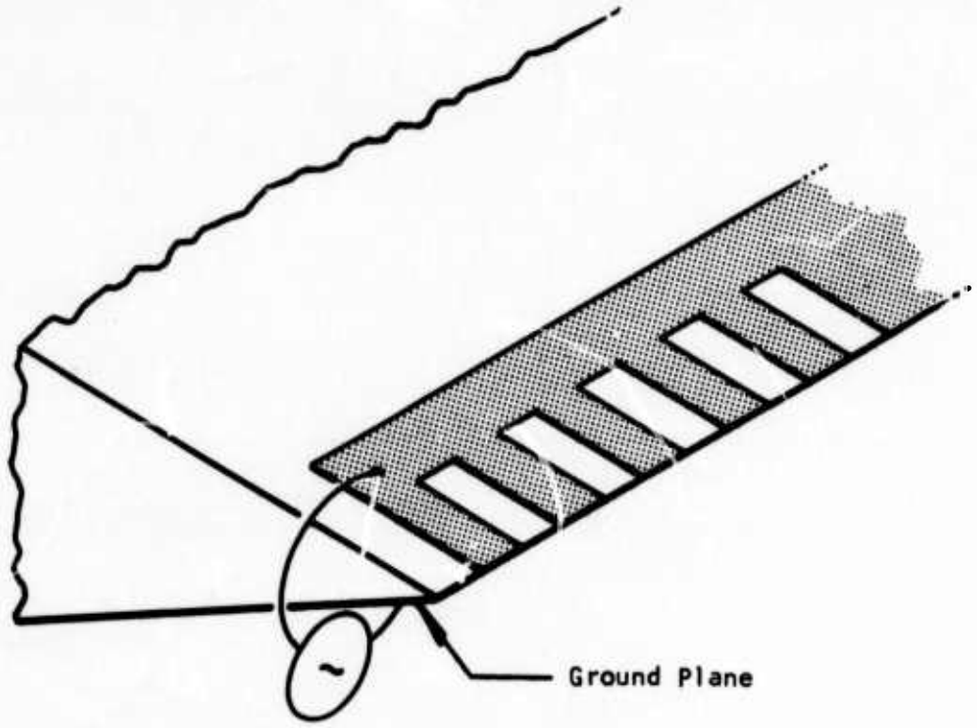

(a)

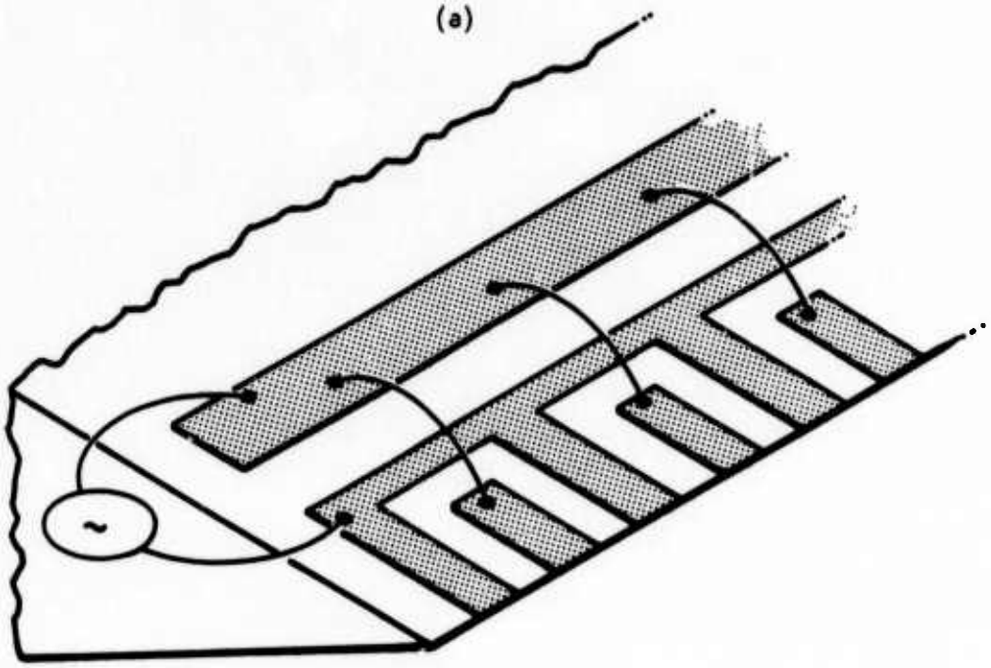

(b)

Figure 3 Transducer Configurations Used in the Prototype Device Evaluation. Figure 3(a) shows a grating mode transducer employing a ground plane. Figure 3(b) shows an interdigital transducer with half the fingers stitch-bonded to one pad.

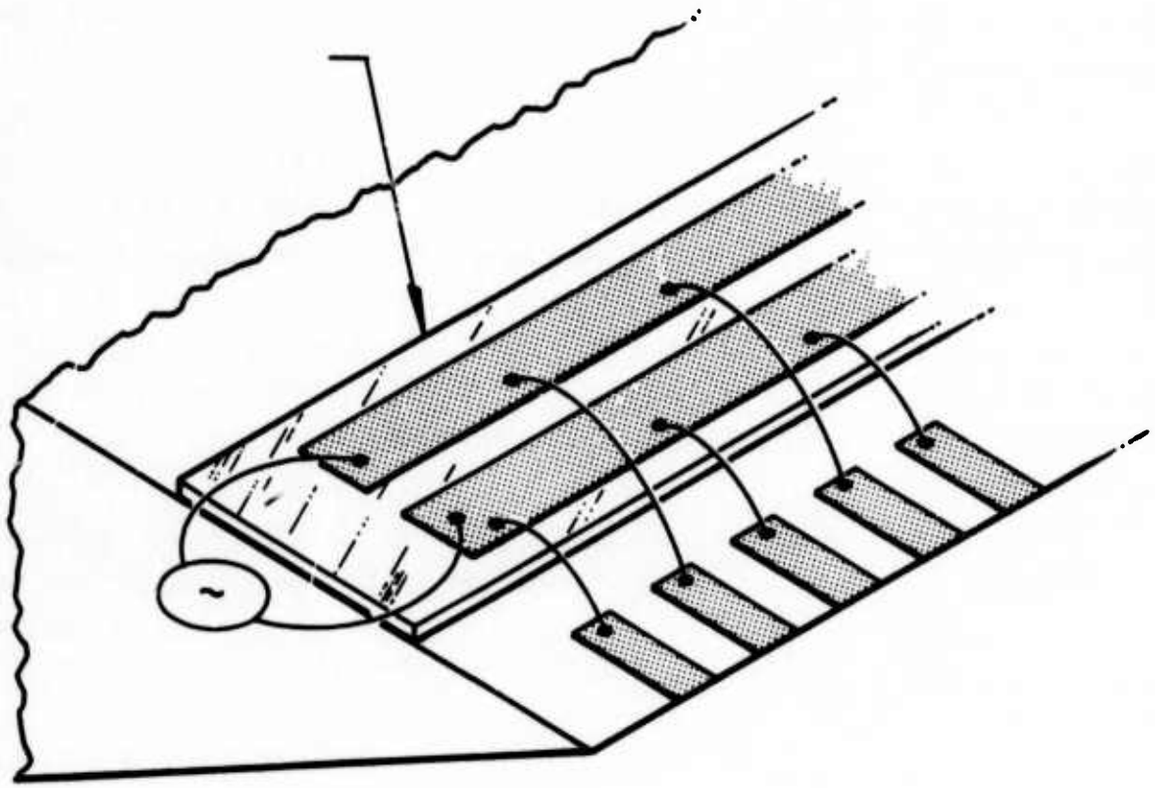

(c)

Figure 3 (continued) Transducer Configurations Used in the Prototype Device Evaluation. In Figure 3(c) the pads are spaced away from the ceramic surface, and all fingers are bonded to the pads.

transducer and the first finger of the output transducer. Waveguiding activity could be observed using either the Figure 3(a) or 3(b) mask, but the observed levels were on the order of -60 dB, which was also the level of transducer pad acoustic crosstalk.

By removing the pads from the substrate as shown in Figure 3(c), acoustic interference effects were virtually eliminated. (Electromagnetic crosstalk was less than -90 dB.) The 9.5 λ interaction length of the transducers was adequate for a strong effect to be observed, as shown by the results of Figure 4. Two modes are clearly visible. The mode at about 1 MHz is the lowest-order antisymmetric flexural mode, while the mode at about 1.7 MHz is the first higher order mode. These modes are indicated as circles in Figure 2.

The deep rejection at the transmission zeros of the fundamental mode shows how thoroughly the acoustic crosstalk in the device is absent. With insertion loss to the peak of the first mode at about -35 dB the average acoustic background level shown in Figure 4 is around -90 dB.

C. Dispersion, Impedances, and Matching Properties

1. Dispersion

Assuming that the transducer fingers are aligned perpendicular to the propagation direction, the transmission zero data of Figure 4 can be used to obtain information about the dispersion of the modes. The frequencies of the zeros of transmission of the two modes were counted and combined with the corresponding Fourier wavelengths of the transducer potential to give the dispersion relations shown in Figure 5. There is not enough data to draw conclusions about the second mode, but the trend for the first mode seems clear. It suggests that over a 47% bandwidth the dispersion is 2.4%.

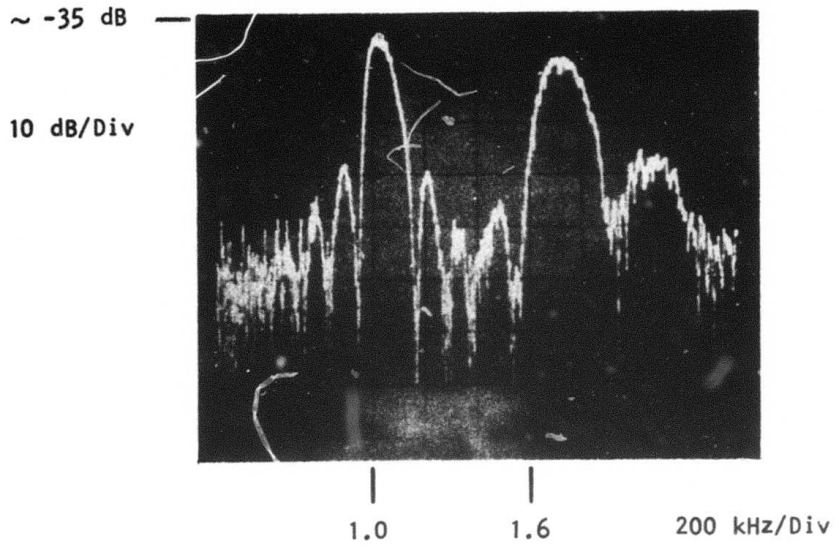

Figure 4 Untuned Insertion Loss of a 33° Ceramic Waveguide. The transducer in Figure 3(c) was used in the delay line.

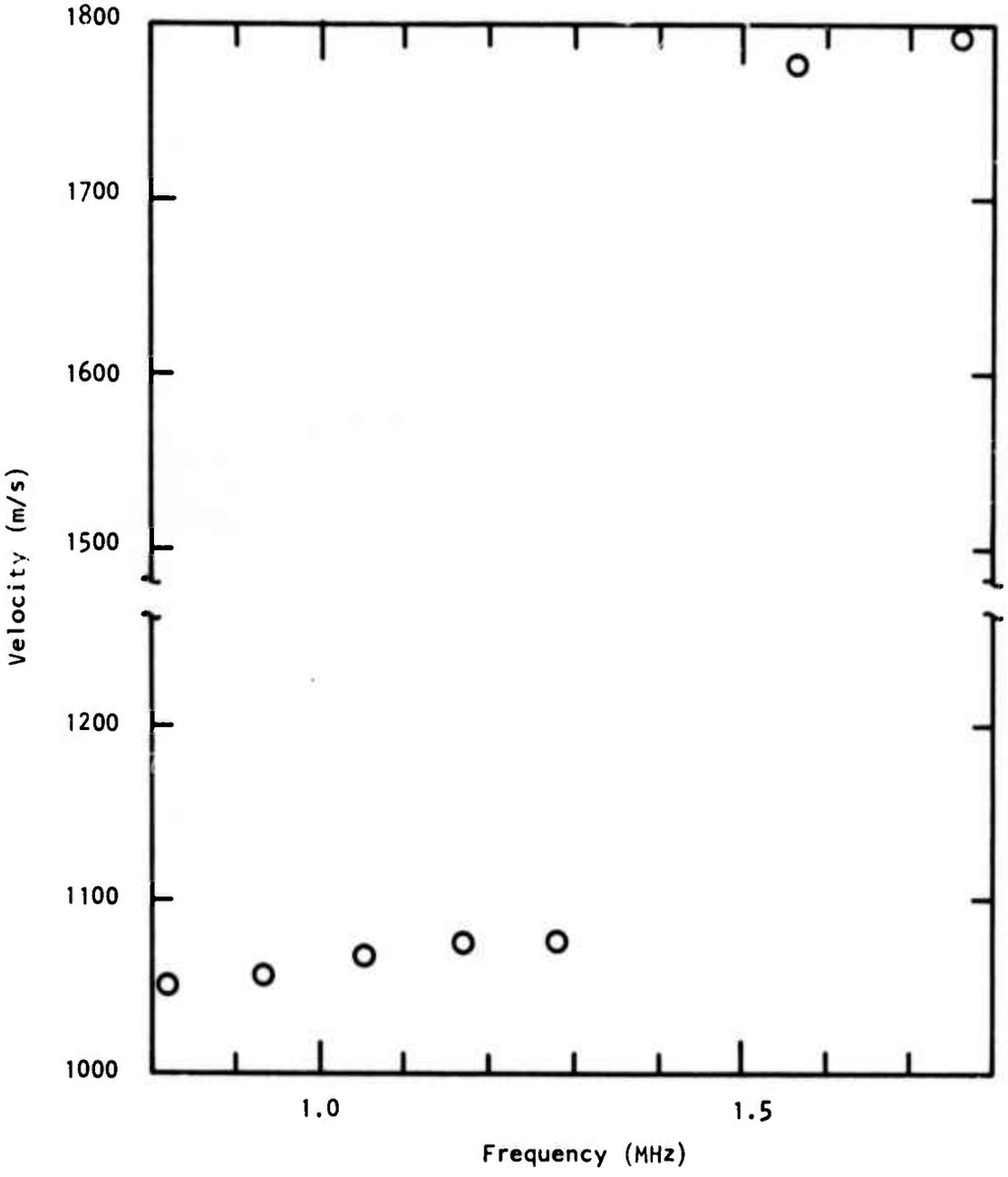

Figure 5 Dispersion Data for the Ceramic Waveguide Shown in Figures 3(c) and 4. The transducer had a 0.040 inch wavelength.

2. Impedances

The transducer shown in Figure 3(c) had 0.010 inch lines and spaces, and the electrodes were approximately $\lambda/2$ long (0.020 inch). Only 9.5 λ of interaction was used, so the static reactance of the transducer was quite large. Low frequency measurements indicated a capacitance of 74 pF, giving a reactance of 2.2 K at 1 MHz. To obtain a Smith chart display of the impedance, the transducer was series-tuned with a 340 μH inductor. The result is shown in Figure 6(a). The loop in the impedance display shows clearly and crosses the real axis at midband with a value of $\sim$ 700 Ω. Minor loops on the main lobe are also evident and are a consequence of reflections from the other transducer, which was not waxed during the measurement.

Insertion loss data for the delay line are shown in Figure 7. The upper photo shows rejection of the second mode due to the series tuning. The fundamental mode has an average insertion loss across the passband on the order of -17 dB. A high degree of interference shows in the lower trace, where the amplitude peak-to-peak is greater than 10 dB. This is a consequence of the high impedances of the transducers, which were series-tuned by an inductor; when they were connected to a 50 Ω spectrum analyzer, triple-transit reflections were very large.

Another surprising characteristic of the frequency response is the very steep skirts on the main passband. These, too, are a consequence of impedance effects. Referring to Figure 6(a) again, one can see that the best impedance match for the fundamental mode occurs at the edges of the passband and that at midband, the impedance match is very poor. These mismatching effects serve to steepen the rejection on the passband skirts.

3. Matching

To overcome the significant impedance mismatch of the waveguide in a 50 Ω system, transformers were added to the matching networks of the transducers.

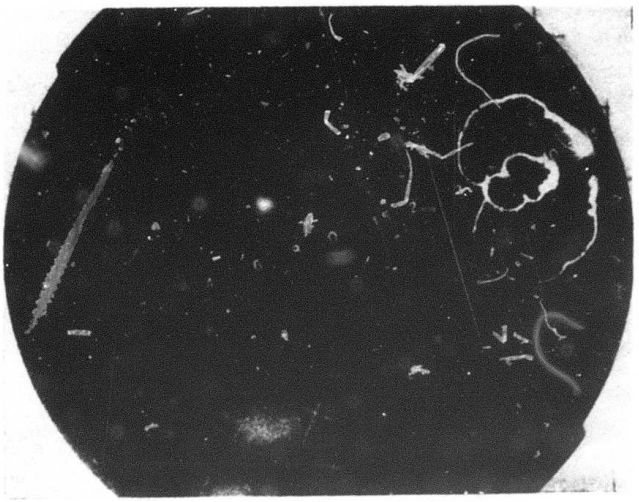

(a)

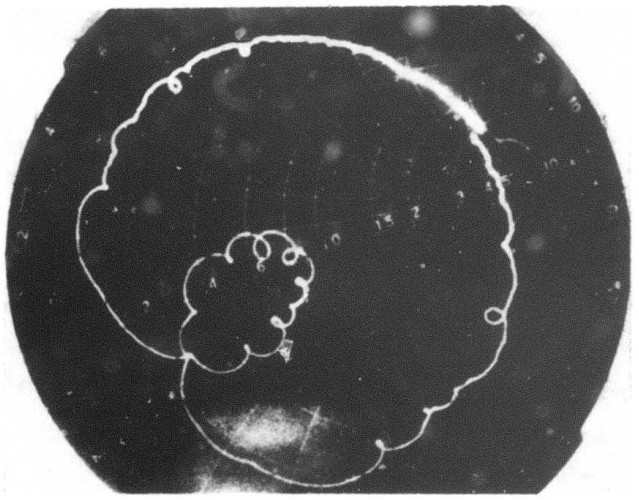

(b)

Figure 6 (a) Impedance of the Transducer After Tuning with a Series Inductor. (b) Impedance Looking into a 16:1 Impedance Transformer in Front of the Series-Tuned Transducer

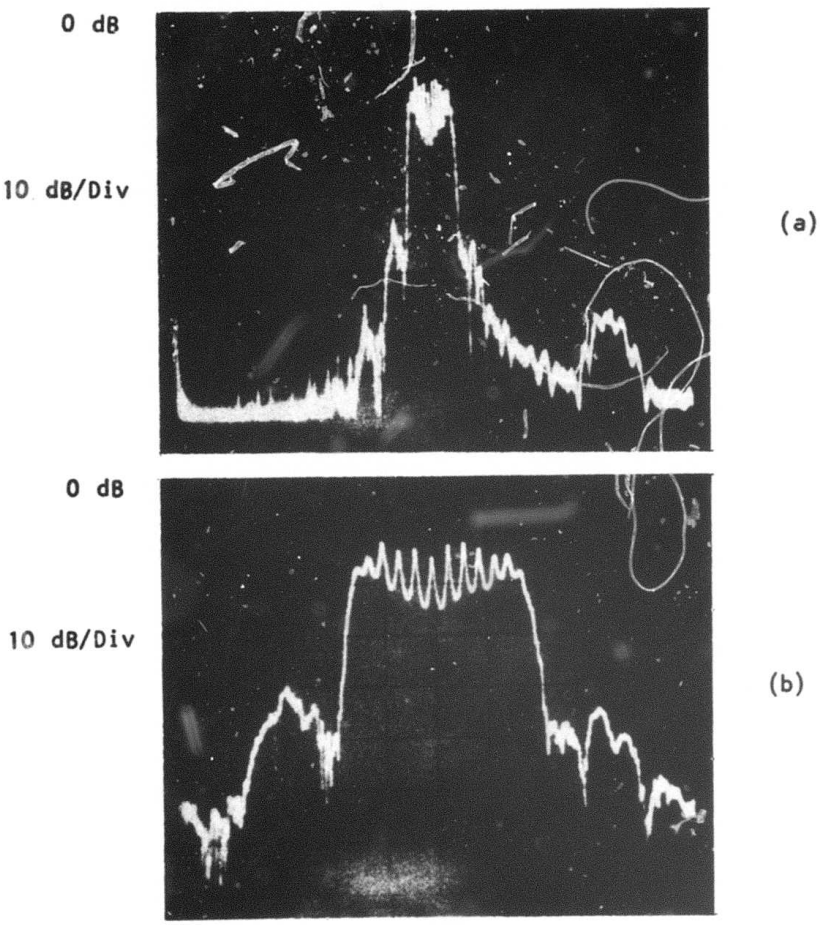

Figure 7 Insertion Losses for the Series-Tuned Waveguide. (a) 200 kHz/Div; (b) 50 kHz/Div.

Relcom BT-9 800 Ω:50 Ω transformers were placed in front of the already series-tuned transducers. Insertion loss characteristics from the input transformer to the output transformer are shown in Figure 8.

The average insertion loss shown is -10 dB in the passband, and the triple transit ripple is now only 3 dB peak-to-peak. In addition, the steep rejection skirts that were on the sides of the main passband now roll off smoothly. Smith chart characteristics looking into a transformer are shown in Figure 6(b). At midband the real part of the impedance reaches a value of 45 Ω, a considerable improvement over the condition shown in Figure 6(a), where the midband value is ~ 700 Ω. Figure 6(b) also shows there is a strong residual acoustic generation level out-of-band of the fundamental waveguide mode. This level shows up in Figure 8(a) as a pedestal of interference at the -55 dB level.

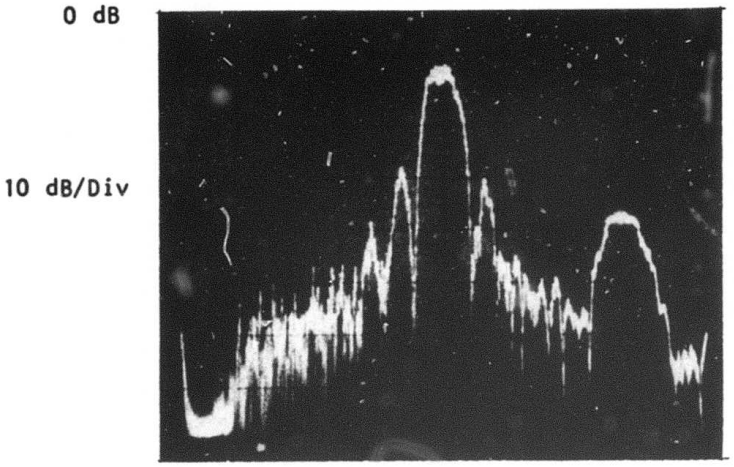

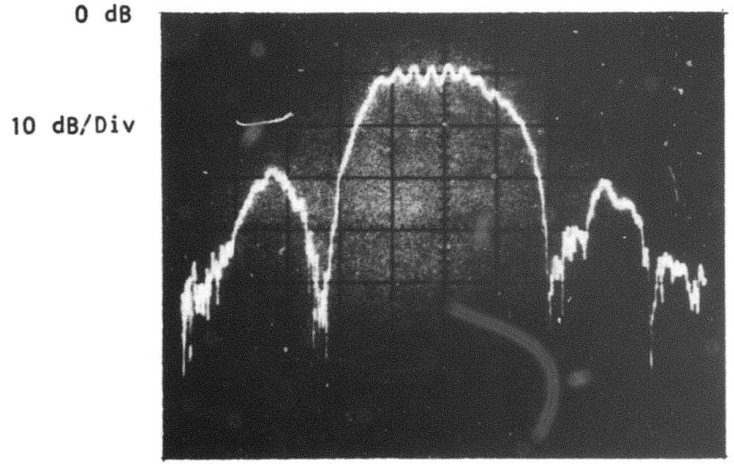

Figure 8 Insertion Losses for the Matched Waveguide. (a) 200 kHz/Div; (b) 50 kHz/Div.

SECTION III

ETCHED WAVEGUIDES

A. Introduction

Previous work carried out by D. F. Weirauch[2] on the correlation of the anisotropic etching of spheres and wafers defined potentially useful orientations of $LiNbO_3$ and α-quartz. These wafer orientations could be etched in HF to produce overhanging wedges with the configuration of Figure 1.

During that work and the present investigation, HF acid was the only etchant given serious examination. It was found that HF etches α-quartz rapidly and produces quite satisfactory waveguides. It etches $LiNbO_3$ nearly an order of magnitude more slowly, and the results, at present, are not satisfactory for wave propagation.

B. α-Quartz Etching

Weirauch found that if the etch mask pattern on standard ST-cut quartz were oriented $\sim 9°$ from the positive X-axis of the crystal, as shown in Figure 9, undercut ledges with top angles on the order of 60° could be obtained. During the course of this work, we have etched many waveguides with orientations near that shown in Figure 9 and have found several other etch planes in addition to the major slow etch plane that defines the lower edge of the waveguide. The presence of these other planes is sensitive to the exact angle of orientation of the waveguide. There is an angle at just about 10° off X where the lower surface of the guide is a single plane. At ± 1° from this direction in the plane of an ST-cut wafer, the lower guide surface became multifaceted.

Figure 10 shows a perspective view of pairs of waveguides on ST-cut quartz. The waveguides are approximately 25 μm high; their lower surfaces are single-faceted, and the apexes are smooth over large propagation lengths. Top angles of these waveguides measured about 60°.

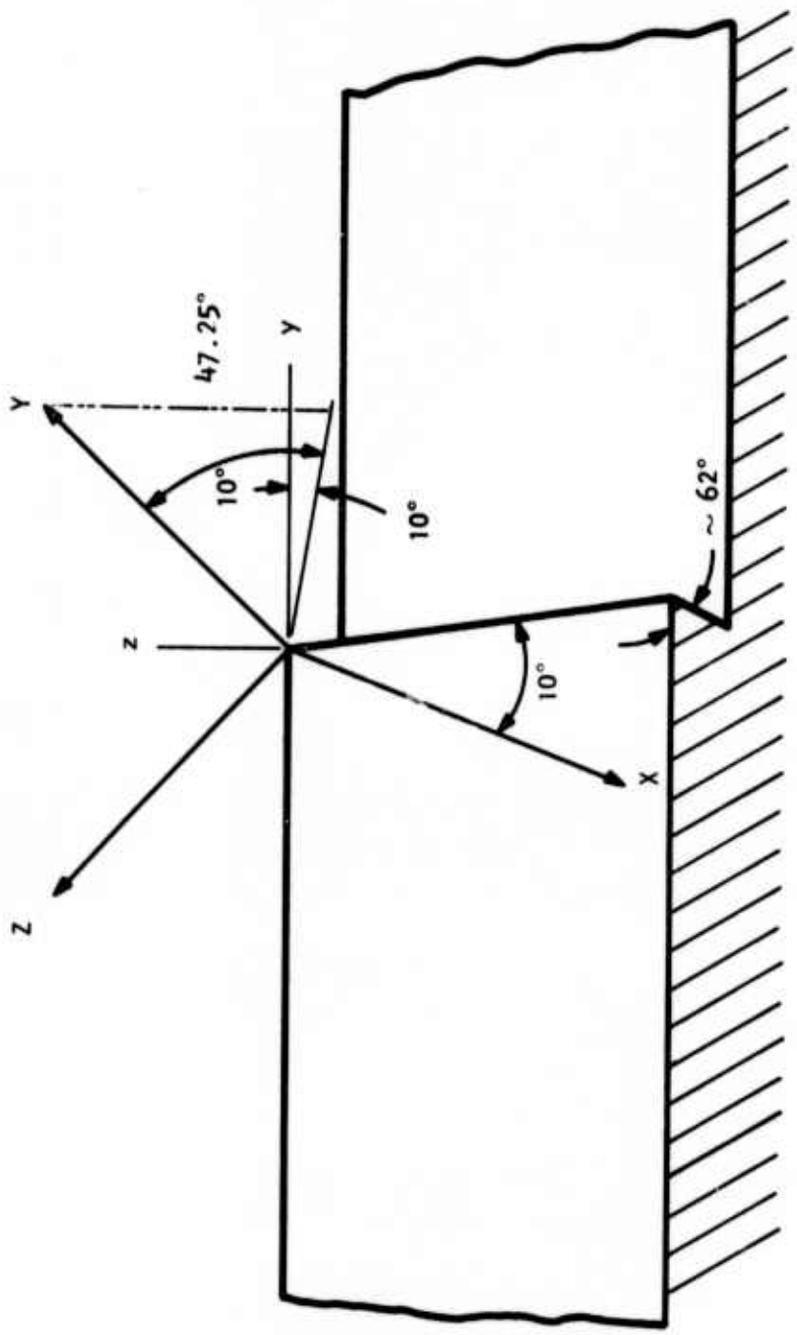

Figure 9 Orientation of an Etched Ledge on ST-Cut Quartz

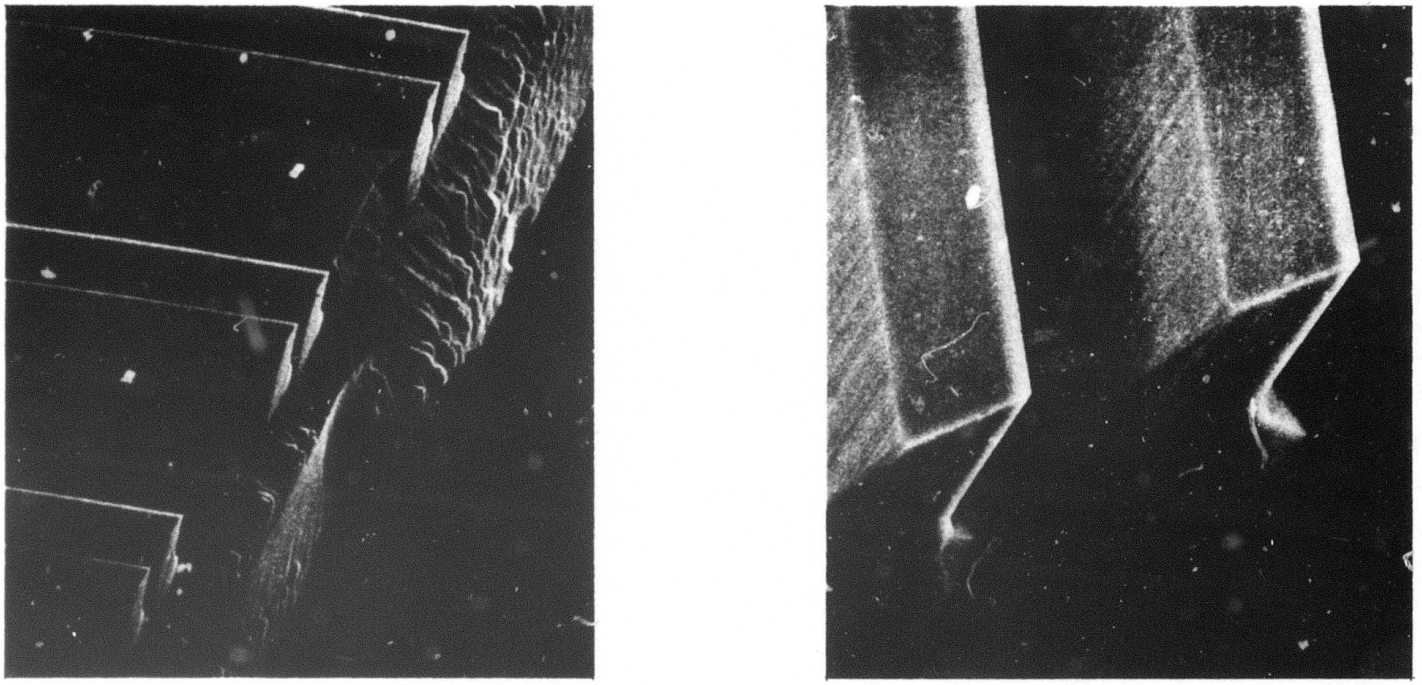

(a) (b)

Figure 10 Waveguides Etched in ST-Cut Quartz. The top angles are 60°. (a) 150X; (b) 700X.

The waveguides were formed by etching in boiling HF for approximately one hour with the surface masked by a chrome-gold pattern. Etch mask erosion was minimal, and defects in the chrome-gold mask were rare, as evidenced by the uniformity of the waveguides.

In general, waveguides with top angles approaching 90° have fundamental mode phase velocities near that of the Rayleigh mode. Accordingly, we have rotated the top surface with respect to the slow-etch lower face of the waveguide to find a wafer orientation that will allow etching of waveguides with top angles near 40°. Figure 11 shows the crystal axes orientation. Wafers with this orientation have been produced and are currently being evaluated.

C. $LiNbO_3$ Etching

1. Experimental Results

Lithium niobate also shows highly anisotropic etching characteristics. Although $LiNbO_3$ permits etching of higher coupling waveguides than does quartz, $LiNbO_3$ fabrication is much more difficult than that of quartz. Slow crystal etch rates and etch mask erosion are the current limitations to achieving high quality $LiNbO_3$ waveguides.

Lithium niobate etches at about one-sixth the rate of quartz in boiling HF. Waveguides with heights on the order of 25 μm require etch times on the order of four hours. At present, our etch masks cannot withstand such a long exposure to boiling HF. The etch mask erodes fastest around actual and incipient defects in the chrome-gold film and near regions of foreign matter at the substrate-film interface. As a consequence, mask erosion is nonuniform, and the waveguides thus formed are ragged along the apex line. Increased emphasis is being placed on etch masking and verification of the crystallinity of the wafer surface, as discussed briefly in Section IV.

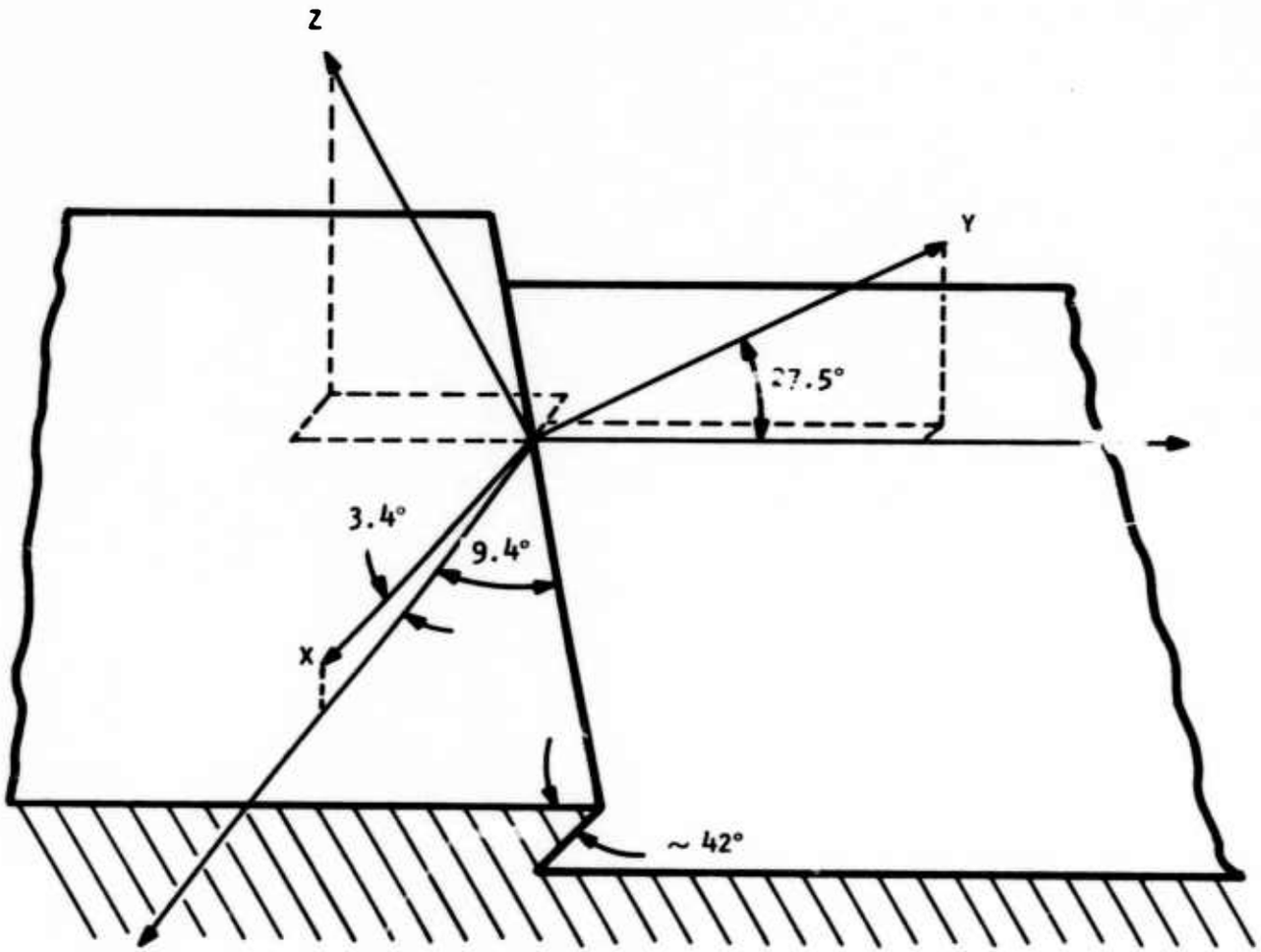

Figure 11 Orientation of α-Quartz That Will Permit Fabrication of Waveguides with 42° Top Angles

Standard YZ $LiNbO_3$ wafers can be etched to produce wedge-shaped waveguides. The polarity of the crystal axes must be determined, however, since they can be etched only on a + Y face. Figure 12 shows the orientation of axes and the resulting cross section from etching X-directed guides. The top angle is $\sim 26°$, and the lower face of the waveguide is ~ 22 μm long. Etching was carried out in boiling HF for three hours. Though the waveguide in Figure 12 was of high quality at the cleavage plane shown, it did not maintain this quality over a long propagation path due to etch mask erosion.

The (YZ) $LiNbO_3$ wafer polarity can be determined readily. The plus and minus Y faces etch in HF at quite different rates and show markedly different structure. Typical results after one hour of etching in boiling HF are shown in Figure 13. Figure 13(a), which shows the highest structure, indicates a face with the -Y axis out of the page. Figure 13(b) shows the +Y face, which etches at one-sixth the rate of the -Y face.

2. Theoretical Results

Analytic characterization of the $LiNbO_3$ waveguides has been carried out. The results, which are presented in Figures 14 through 16, show that the theoretical characteristics of the waveguide are excellent. The analysis was performed using the computer program developed by P. E. Lagasse. Finite element solutions were found for many wedge-shaped $LiNbO_3$ structures, all of which had a lower guide surface coplanar with the slow etch plane about 26° down from the +Y surface. In the calculations, variation of the apex angle, θ, meant moving the upper surface of the waveguide while keeping the lower surface with a constant crystal orientation. All the guides analyzed were 6 λ from fixed base to apex.

Phase velocity data for the first two modes are shown in Figure 14. At $\theta = 26°$, corresponding to the etching of a (YZ) $LiNbO_3$ wafer, the fundamental mode velocity is on the order of 1600 m/s. Rayleigh wave velocity on (YZ)-$LiNbO_3$

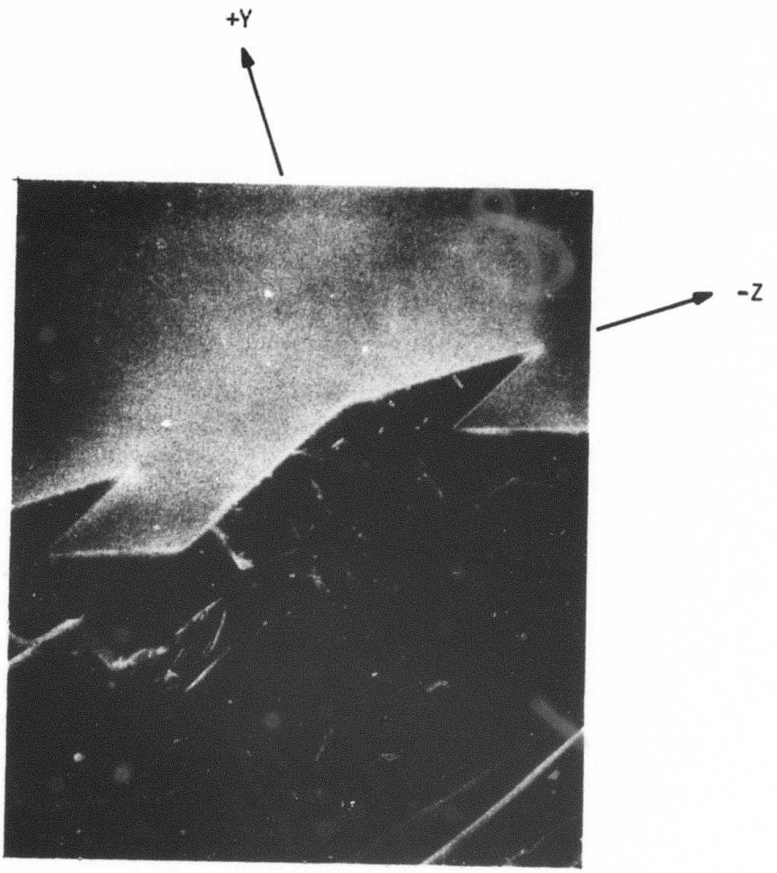

Figure 12 Etched $LiNbO_3$ Waveguides. Cross-sectional view at ~ 800X.

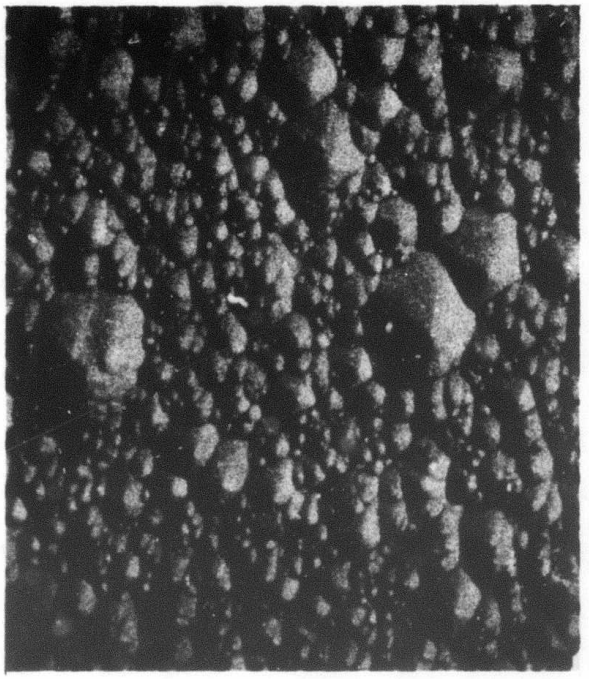

-Y - face

(a)

+Y - face

(b)

Figure 13 Y-Faces of $LiNbO_3$ Etched in Boiling HF Acid for One Hour. The slow etching +Y face permits wedge waveguide fabrication.

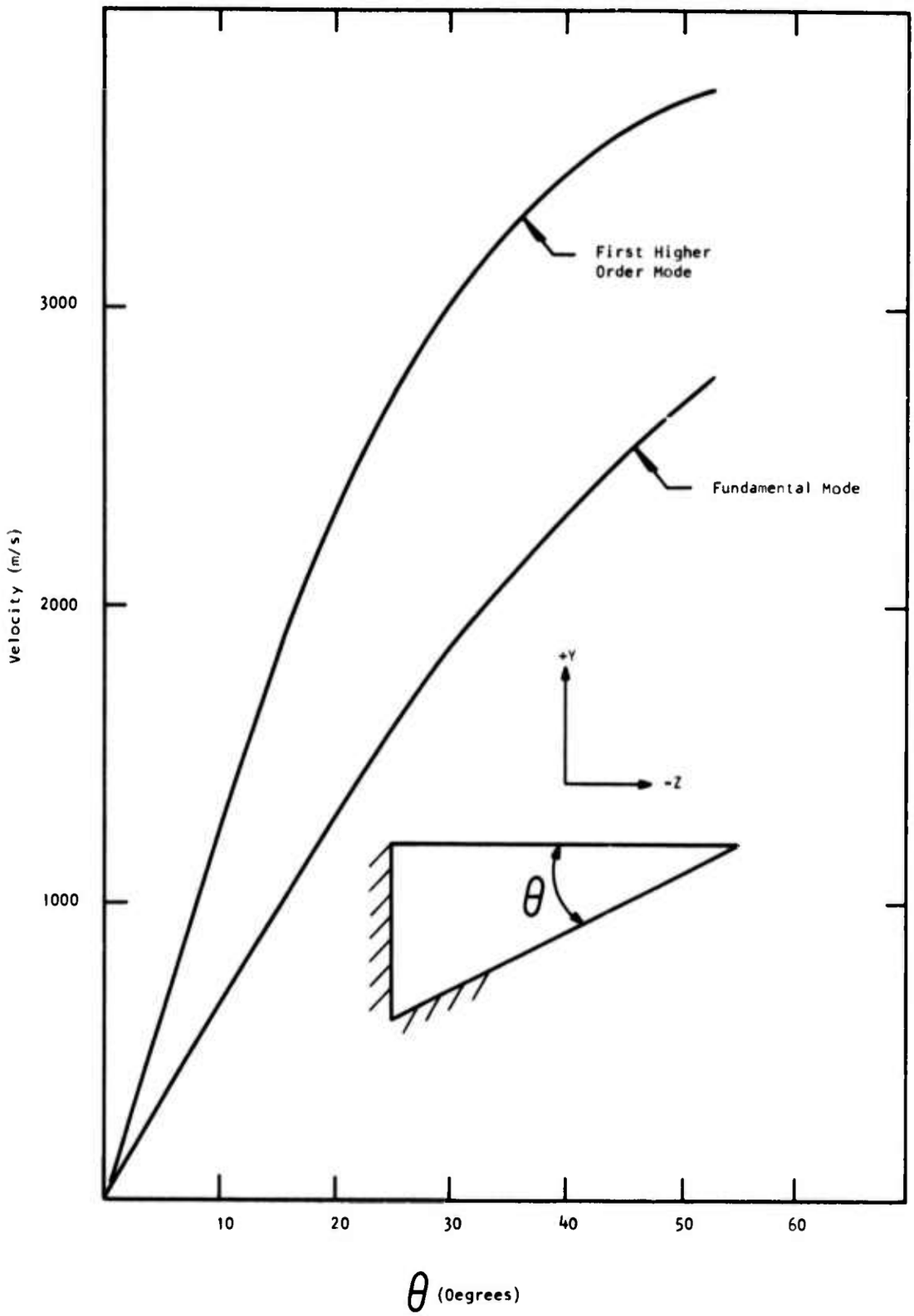

Figure 14 Phase Velocities for the First Two Modes of a $LiNbO_3$ Waveguide

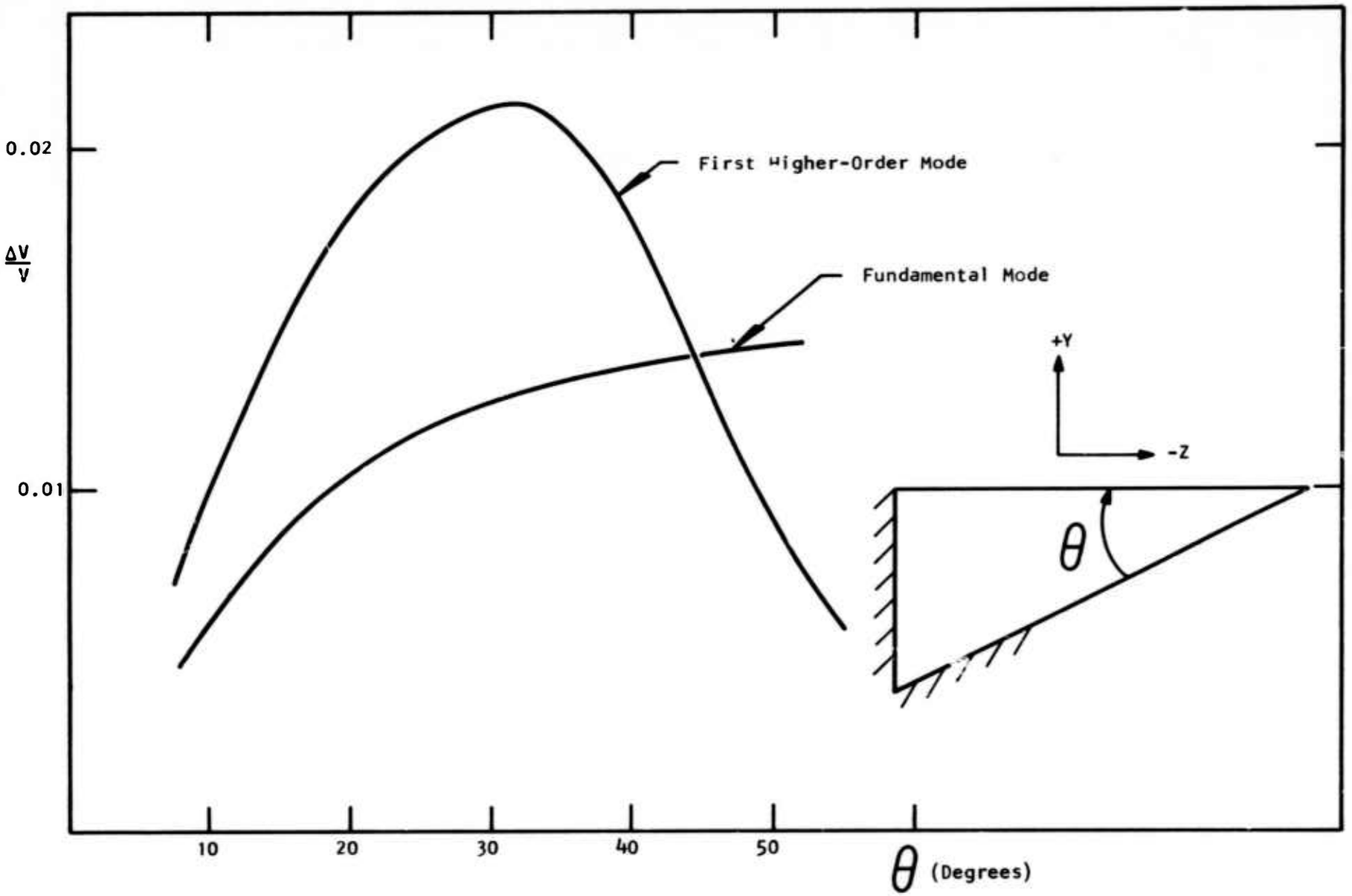

Figure 15 Coupling Parameters for the First Two Modes of a $LiNbO_3$ Waveguide

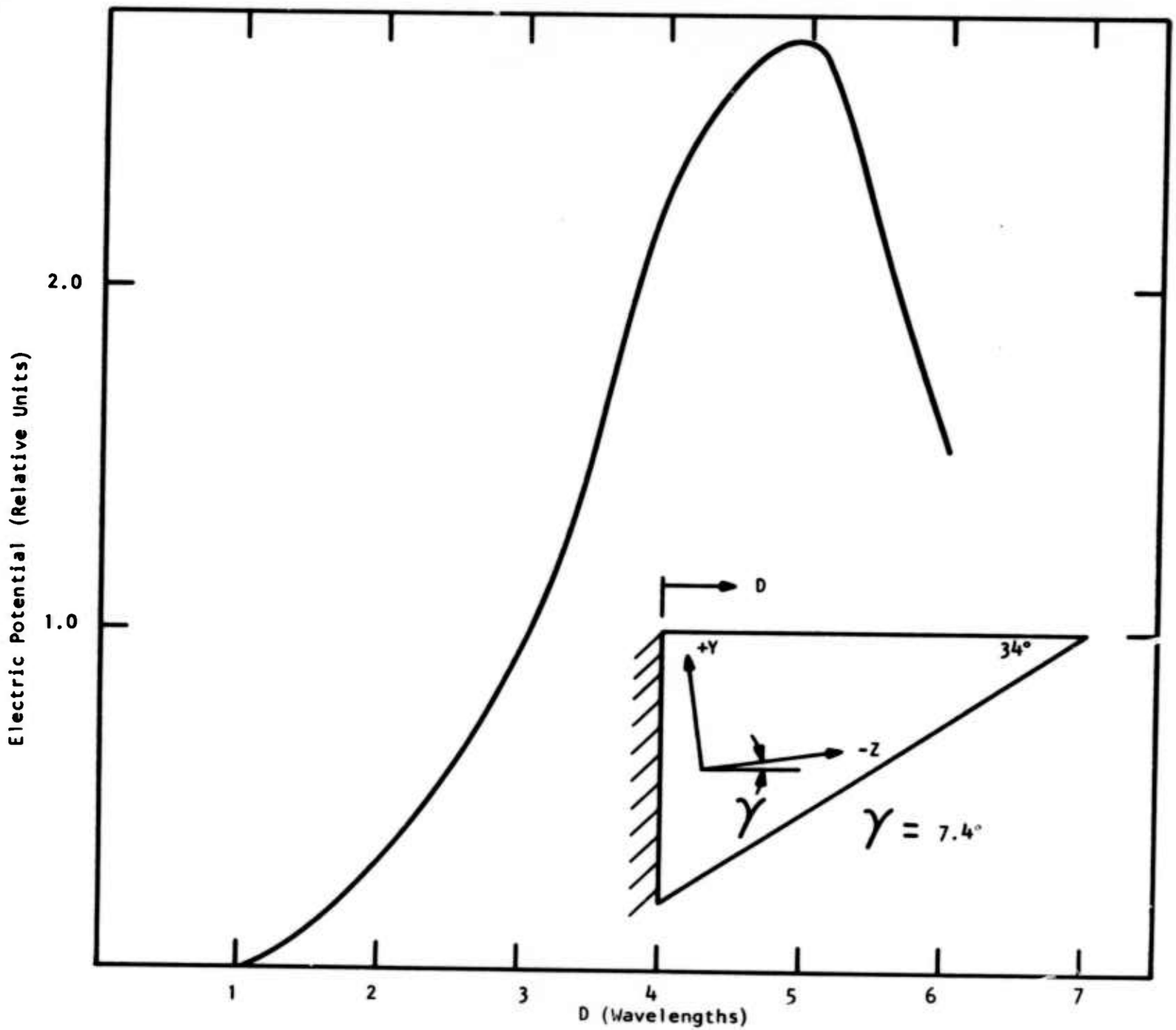

Figure 16 Electric Potential Along the Surface of a $LiNbO_3$ Waveguide with a Top Angle of 34°

is 3488 m/s. The first higher-order mode, which is the only potentially interfering mode, is about 70% higher in velocity. Of course, this puts it well out of band of most fundamental mode applications.

The slope of the phase velocity curve is quite steep everywhere and at $\theta = 26°$ is 53 m/s per degree. Consequently, errors in orienting the +Y surface lead to center frequency errors of 9 parts per million per second of arc.

Coupling calculations for the first two modes of the $LiNbO_3$ waveguide are shown in Figure 15. The coupling to the fundamental mode increases rapidly with angle to greater than 1%, after which it increases slowly. At 26° the fundamental mode coupling is 1.2%, half as much as coupling to the Rayleigh mode on (YZ)-$LiNbO_3$.

Perhaps the strong coupling could have been anticipated because of the high piezoelectricity of $LiNbO_3$. However, we did not expect, and were very pleased to discover, the long distance along the top surface of the guide in which the electric potential is of one sign. Figure 16 shows the electric potential for a $LiNbO_3$ waveguide with a 34° top angle. The plot shows that at least three wavelengths along the top surface can be used for transducer fabrication. This represents a significant relaxation in the transducer impedance problems encountered in making one-half wavelength wide transducers. However, the level of acoustic activity along the guide surface away from the apex shows that, for dispersionless operation, the waveguides should be etched several wavelengths deep. Additional etching would require longer etch times, worsening the etch mask erosion problem.

SECTION IV

FUTURE WORK

During the next contract period, greater emphasis will be given to evaluation of the etch mask erosion problem. Other masking materials will be considered, and film application and substrate clean-up techniques will be examined. Data indicate that the raggedness observed in etched $LiNbO_3$ waveguides may be due to crystal defects; whether these defects are from crystal growth or are induced during wafer preparation is not known. We will examine both possibilities by obtaining materials from different vendors as well as by evaluating prepared wafers for single crystallinity of the polished surface.

Finally, work on silicon stencil fabrication will continue in preparation for monolithic transducer fabrication on $LiNbO_3$ waveguides. Assuming that the etch mask erosion problem can be overcome, we now expect that 10 to 30 MHz etched $LiNbO_3$ waveguide operation will be accomplished within the next three to four months.

ACKNOWLEDGMENT

The computer program used for the finite element calculations was obtained from P. E. Lagasse.

REFERENCES

1. R. C. Rosenfeld and K. E. Bean, "Fabrication of Topographical Ridge Guides on Silicon for VHF Operation," Proc. IEEE Ultrasonics Symposium, Boston, Mass., pp. 186-189 (October 1972).

2. D. F. Weirauch, "The Correlation of the Anisotropic Etching of Single Crystal Silicon Spheres and Wafers," J. Appl. Phys. 46, 4, 1478-1483 (April 1975).

3. E. J. Staples, "High Resolution SWD Pattern Replication Without Photo-Chemical Processing," Proc. IEEE Ultrasonics Symposium, Monterey, Calif., pp. 522-524 (November 1973).

4. P. E. Lagasse, I. M. Mason, and E. A. Ash, "Acoustic Surface Waveguides - Analysis and Assessment," IEEE Trans. Microwave Theory and Techniques MTT-24, 4, 225-236 (April 1973).